2024, 21(10): 3277-3288
https://doi.org/10.21123/bsj.2024.10452
P-ISSN: 2078-8665 - E-ISSN: 2411-7986
Baghdad Science Journal

Comparison of physical characteristics of mass and luminosity function of disk systems in barred and unbarred spiral galaxies

Al Najm M.N.**, Y. E. Rashed, H. H. AL-Dahlaki

Department of Astronomy and Space, College of Science, University of Baghdad, Baghdad, Iraq.
*Corresponding Author.

Received 14/12/2023, Revised 05/02/2024, Accepted 07/02/2024, Published Online First 20/03/2024, Published 01/10/2024

Abstract

Among the most important ways to investigate galaxies' distribution over cosmic time is the luminosity function LF in terms of baryonic disc mass $\psi^S(M_b)$, magnitude $\emptyset^{\boldsymbol{B}}(\boldsymbol{M_B})$. We have studied an estimate of the baryon mass density in the sample of barred and unbarred spiral-type galaxies from previous literature, which virtually involves, for each class of objects with visible baryon content, an integral over the luminosity of the product of the luminosity function (LF) and the mass-to-light ratio. The multiple regression technique used the statistical software package in our study and results, such as database analysis and graphing software (Statistics Win and Origin Pro programs). According to the statistical analysis, there is a strong positive and very relevant correlation ($\emptyset^{\boldsymbol{B}}(\boldsymbol{M_B})$, $\boldsymbol{\psi^S}(\mathbf{M_b})\alpha\ M_B^{\sim 1}$), and both barred and unbarred disc spiral galaxies often exhibit M_B < -18 mag. The "knee" of the luminosity function for spiral galaxies shows a large cutoff at the baryonic mass of $M_b > 10^{10}\ M_\odot$ for barred and unbarred spirals. These provide evidence supporting the hypothesis that disc system spirals began to form inside an increased mass threshold. Since the increase of the star's initial mass function with redshift is much more rapid, our findings have indicated that the comoving initial mass function $\psi^S(M_b)$ of barred and unbarred galaxies at elevated redshift (z > 0.027 for barred and z > 0.02 for unbarred) appears to be declining compared to the critical universe.

Keywords: Baryonic mass; Initial mass function; Luminosity function; Spiral-type galaxies; Atomic and molecular gas.

Introduction

Bars and spirals share morphological identifications, they play featured roles within galaxies' dynamics. Bars are often known as significant components driving galactic dynamics, while spirals are believed to have potential outcomes influenced by the presence of bars. Many ordinary galaxies lack bars while still showing spiral features. The significance of bars and spirals in galaxies' long-term evolution cannot be excessive. Barred galaxies can be regarded as the peak of galaxy morphology, organized by highly clear structures. In such galaxies, the presence of a bar represents a prominent disturbance. On the other hand, galaxies devoid of these driving mechanisms typically do not exhibit long-term evolution. These include unbarred galaxies featuring classical bulges and minimal or absent global spiral patterns. Both barred and unbarred galaxies may show outer rings, typically located at roughly double the radius of the inner disk. Unbarred galaxies typically possess intrinsic pivotal ratios of

2024, 21(10): 3277-3288
https://doi.org/10.21123/bsj.2024.10452
P-ISSN: 2078-8665 - E-ISSN: 2411-7986
Baghdad Science Journal

approximately 0.85 for their inner disks. Bars, on the other hand, present greater extension, with typical axial ratios of approximately 0.2, but only a smaller portion, typically less than one-third of the disk, participates in forming bars [1-3]. In a modern analysis involving H-band (1.65 μm) images of 186 bright galaxies, 56% were visually categorized as 'strongly barred,' 16% as 'weakly barred,' and 27% as 'unbarred in the near-infrared [4, 5]. Bars in spiral galaxies exhibit different morphologies and non-elliptical shapes. These elongated linear structures within galaxies' central regions result from disc instabilities and the redistribution of angular momentum within the disc. A typical normal bar in an early-type galaxy consists of two segments: a broad inner region and narrower ends. Barred galaxies and those dominated by bulges tend to be fixed in denser environments compared to their unbarred counterparts, which have predominantly disk-like structures [6].

Comprehending the intricacies of galaxy formation and evolution remains in its early stages, and a comprehensive framework that fully elucidates the processes governing how galaxies emerge and transform into their current structures has yet to be fully elucidated. A classical approach involves leveraging the statistical characteristics of galaxy properties across various galaxy populations [7, 8]. In many realms of astronomy and cosmology, a commonly employed tool for scrutinizing the statistical attributes of object populations is the analysis of luminosity and mass functions. Mass functions (MFs) associated with stars and gas play a key role in studying the physical means that guide the formation and evolution of galaxies. These functions depict an essential cornerstone of improving theories through experimental observations [9, 10]. During the Big Bang, approximately 5% of the generated mass materialized as normal baryonic matter composed of neutrons and protons. Of this fraction, approximately 10% eventually assemble to form star-shaped galaxies or various gaseous states, which can contain molecular, atomic, or ionized states[11-14].

Salucci and Persic[15] computed the baryonic mass function, defined as $\psi^s(M_{bayronic})$, for disc system galaxies. They utilized reliable luminosity functions and baryonic mass-to-light ratios in their analysis. Their findings revealed that the baryonic mass function of disc systems can be approximated as a power law $\psi^s(M_{bayronic}) \alpha M_{bayronic}^{-1/2}$, where this relationship holds from 10^8 to $2x10^{11}$ solar masses ($M_\odot$). However, a distinct abrupt cut-off point is observed due to the scarcity of objects beyond this range. Shankar, et al [16] derived the Baryonic Mass Function (BMF) for galactic structures by examining their inner kinematics. They ensure its cosmological significance by demonstrating its universal character. Their research establishes a connection between a galaxy's baryonic mass and its virial (total, dark) mass. Generally, this study underscored the influence of baryonic feedback mechanisms, such as supernova explosions and quasar activity, in linking dark and ordinary matter within galaxies. In a prior investigation conducted by Read, and Neil [17] measured the baryonic mass function of galaxies, providing insights into how baryonic mass is distributed among different types of galaxies (e.g., spiral or elliptical) and various size categories, their study developed in the conclusion that a significant portion of the Universe's baryons exist outside of galaxies, likely residing within the warm/hot intergalactic medium (WHIM). In 2008, Kevin et al [18] presented estimates of low-mass stars' luminosity and mass functions, drawing from the SDSS/2MASS data catalog. Their investigation revealed that the logarithmically binned mass function best conforms to a log-normal distribution with a peak at Mc = 0.29, encompassing a 90% confidence interval ranging from Mc = 0.20 to 0.50. This translates to linearly binned mass functions peaking between 0.27 $M_\odot$ and 0.12 $M_\odot$.

Trachternach et al [19] investigated the relationship between baryonic mass and maximum rotation velocity using the baryonic Tully-Fisher relation "BTF". Their concluded results found the significance of the Baryonic Tully-Fisher (BTF) relation as a fundamental link connecting the visual, baryonic matter, and dark matter masses within galaxies. Amanda et al [20] initiated a study of the galaxy cosmological mass function "GCMF" using a semi-empirical relativistic system, employing observational data drawn from current galaxy redshift surveys. Their research outcomes corroborated that the "GCMF" adheres to the theoretical expectations derived from cold dark matter models, wherein less massive objects are formed first, followed by the emergence of more massive counterparts.

Hunt et al [21] established an exploration of the evolution of the number density of Luminous Compact Blue Galaxies (LCBGs) within the redshift range $0.1 \leq z < 1.0$. Specifically, their study featured

2024, 21(10): 3277-3288
https://doi.org/10.21123/bsj.2024.10452
P-ISSN: 2078-8665 - E-ISSN: 2411-7986
Baghdad Science Journal

a consistent and extensive dataset, encompassing a sample of LCBGs nearly two orders of magnitude larger than any previous investigation. Their research unveiled that "LCBGs" contribute approximately 48% of the luminosity density exhibited by galaxies with luminosities greater than $M_B = -18.5$ at a redshift of approximately $z \sim 0.88$. Moreover, their findings indicated that the number density of LCBGs develops as $N = (7.3 \pm 0.2 \times z + 0.1 \pm 0.1) \times 10^{-3} h_o^{-3} Mpc^{-3}$.

Materials and Methods

Sample collections and databases

This work is established on the data group gathered from the NASA/IPAC Extragalactic Database (NED) surveys [22-24], which is supported by the National Aeronautics and Space Administration and operated by the California Institute of Technology, such as Hubble luminosity distance (d_L) of the Cosmic Microwave Background "CMB", and the velocity-integrated intensity S_{CO} (for the transition J=1-0) in the unit (Jy. km/s). The apparent magnitude (*Btc*) in the blue band is corrected by (galactic extinction "*ag*", internal extinction "*ai*" and k-correction "*ak*"), absolute magnitude M_B in the blue band, which is computed from the correct magnitude *Btc* and the distance modulus μ_{dz} from the redshift or μ_0 redshift-independent (for nearby galaxies $M_B = Btc - \mu_0$, and a more distant galaxies $M_B = Btc - \mu_{dz}$) , and the neutral hydrogen HI flux S_{HI} in 21-cm line profile ($m_{21} = -2.5\, Log\, S_{HI} + 17.4$) appointed from the HyperLEDA database, which is the Observatoire de Lyon "France" and the Special Astrophysical Observatory "Russia" [25, 26]. Furthermore, the data that has been involved in this research was collected from our previous study [27]. The names of the barred and unbarred spiral galaxies, redshift *z*, and their morphological type, and these parameters are offered in Tables (1 and 2) [27].

Statistical procedure

The link between several independent or predictor variables and an associated or criterion variable is explored further in multivariate regression. One dependent (criterion, endogenous) variable is associated with many independent (predictor, exogenous) variables in an orderly multiple regression study, computed using the multiple regression module. The multivariate regression equation is extremely significant generally (for an explanation of statistical significance testing, see Elementary Basics). So, it is possible to "predict" impoverishment better than what might have been anticipated by pure chance independently given the variables that are not dependent. An indicator of the relationship between any numbers of variables is a correlation. Interval scales should be used as a minimum for measurements. However, additional correlation coefficients are available to accommodate different kinds of datasets. The range of coefficients of correlation extends from -1 to +1. A perfectly negative correlation is denoted by a value of -1, whereas a perfect positive correlation is expressed by a value of +1 [26, 27]. The associations between the corresponding independent and dependent variables after accounting, for all other factors are called partial correlations. After accounting for all independent variables, it is the correlation between the leftovers. The partial relationship shows each independent variable's distinctive contribution to the dependent variable's estimation. The statistical software programs (such as Statistics Win and Origin Pro) that we utilized for analyzing databases and plotting our investigation and outcomes were employed in the multiple regression techniques.

The mass and luminosity function of spiral galaxies

The luminosity function (LF) is a fundamental tool in examining galaxy evolution. A challenge in determining the LF lies in assembling a sample of galaxies located at the same distance. Therefore, investigating clusters of galaxies, where all galaxies share a common distance, becomes valuable, albeit at the cost of focusing on a specific region of the cosmos [17]. Current cosmological research is driven by a quest to comprehend the origins and development of the structures that have given rise to the galaxies we observe today [28-31]. The LF, represented as Φ(L) and measured in units of ergs s^{-1} Mpc^{-3}, stands as a pivotal tool for exploring the distribution of galaxies across cosmic epochs [10].

The calculation of the Universe's baryon mass density essentially entails integrating, for each class of objects with visible baryon content, the product of the luminosity function (LF), denoted as *Φ(L)*,

2024, 21(10): 3277-3288
https://doi.org/10.21123/bsj.2024.10452
P-ISSN: 2078-8665 - E-ISSN: 2411-7986
Baghdad Science Journal

luminosity *(L)*, and the mass-to-light ratio for the baryon component, M_b/L. This is expressed as [32, 33]:

$$dN = \sum_T \int \Phi(L)\ L\ \left(\frac{M_{baryonic}}{L}\right) dL \ \ldots..1$$

where "*dN*" is the surveyed number of galaxies within a luminosity range [*L, L+dL*], and *T* represents spiral galaxies, clusters, and superclusters.

The overall distribution of galaxies on a global scale can be approximated using the Schechter luminosity function (LF). Initially derived in the form of a mass function during investigations into structure formation and evolution, this function is generally expressed in the following form [10, 32-34]:

$$\emptyset(L) = \frac{\emptyset^*}{L^*}\left(\frac{L}{L^*}\right)^{\alpha} exp\left(-\frac{L}{L^*}\right) \ldots\ldots\ldots\ldots 2$$

Here L^* is characteristic luminosity, (L) is a galaxy luminosity, the normalisation coefficient for the density in the unit ($h^3\ Mpc^{-3}$) is ($\emptyset^*$), the incline of the luminosity function for small stars (L) is α, and ($\emptyset$) is the total number of galaxies per unit volume in (Mpc^{-3}) per unit luminosity function [33].

Estimating the Schechter Luminosity Function in the Blue band (λ=4400Aº)

At this step, it is emphasised that using the straightforward relation in Eq. 2, absolute brightness L is often converted to absolute magnitudes M [10, 27]:

$$M - M^* = 2.5\ log\frac{L}{L^*} \ldots\ldots\ldots\ldots\ldots 3$$

or in the form:

$$L = 10^{-0.4(M-M^*)}.L^* \ldots\ldots\ldots\ldots\ldots\ldots 4$$

By using a standard rule mathematically $\frac{d}{dx}\left[\beta^{u(x)}\right] = Ln(\beta).\beta^{u(x)}u^x$, where (β) is the real number. Eq. 4 is written as follows:

$$\frac{dL}{dM} = \frac{d}{dM}\left[10^{-0.4(M-M^*)}\right].L^*$$

$$\frac{dL}{dM} = ln_{10}\left[10^{-0.4(M-M^*)}\right].(-0.4).L^* \ldots..5$$

We have an interval (dL) in luminosity that corresponds to an interval (dM) in absolute magnitude [33]:

$$\emptyset(M)dM = \emptyset(L)d(-L) \ldots\ldots\ldots\ldots\ldots 6$$

or in the shape:

$$\emptyset(M) = -\emptyset(L)\frac{dL}{dM} \ldots\ldots\ldots\ldots\ldots\ldots 7$$

Substituting Eqs. 2 & 5 into Eq. 7 gets:

$$\emptyset(M) = -\left(\frac{\emptyset^*}{L^*}\right)\left(\frac{L}{L^*}\right)^{\alpha} exp\left(-\frac{L}{L^*}\right).(-0.4).L^*.ln_{10}.10^{-0.4(M-M^*)} \ldots..8$$

So, Eq. 8 can be rewritten in the structure:

$$\emptyset(M) = 0.4\ ln_{10}\ \emptyset^*.10^{-0.4(M-M^*)}.\left(\frac{L}{L^*}\right)^{\alpha}\left(-\frac{L}{L^*}\right) \ldots\ldots\ldots 9$$

Finally, by substituting Eq. 4 $\left(\frac{L}{L^*}\right)$ into Eq. 9, obtains:

$$\emptyset(M) = 0.4\ ln_{10}.\emptyset^*.10^{-0.4(\alpha+1)(M-M^*)}.e^{10^{-0.4(M-M^*)}} \ldots.10$$

In the Blue band at λ=4400Aº, Eq.10 is given by:

$$\emptyset^B(M_B)[\ in\ Mpc^{-3}mag.^{-1}\ ] = 0.92\ \emptyset^*{}_B.10^{-0.4(\alpha_B+1)(M_B-M^*{}_B)}.e^{10^{-0.4(M_B-M^*{}_B)}} ..11$$

As mentioned in Eq. 11 above, this paper adopted a typical set of parameters in the blue band as reported in [33]:$\emptyset^*{}_B = 1.6\times10^{-2}h^3\text{Mpc}^{-3}$, $\alpha_B = -1.07$, $L_B^* = 1.2\times 10^{10}h^{-2}L_{\odot,B}$ is the selected blue waveband's luminosity, M_B^* =*-19.7+5logh* ,h is the degree of uncertainty for calculating H_0, where $h = \frac{H_0}{100}kms^{-1}\ Mpc^{-1} = 0.678\ kms^{-1}\ Mpc^{-1}$, if a constant Hubble $H_0 = 67.8\ kms^{-1}\ Mpc^{-1}$ from the NED website.

The disk system fraction, which refers to the percentage of stars in a star cluster with system disks, is often used to study the formation and evolution of protoplanetary disks. This fraction can be influenced by factors such as the star cluster's age and the system disk's mass distribution. The disk system's primary mass function "DMF" can greatly affect the disk fragment time variability [35]. To understand this, we can calculate the initial luminosity function $\psi^S(M_B)$, which tells us how many stars of magnitude *M* in the interval ΔM_B have formed in spiral galaxies per pc^3 during their existence. The disk systems mass function is defined as the fractional number of disks with mass between $\psi^S(M_b)$ and $\psi^S\ (M_b)\ dM_b$ [15].

$$\Psi^s(M_b)dlogM_b = \phi^s\left(L_B(M_b)\right)\frac{dL_B}{dM_b}dlogM_b \ \ldots\ldots\ldots\ldots 12$$

2024, 21(10): 3277-3288
https://doi.org/10.21123/bsj.2024.10452
P-ISSN: 2078-8665 - E-ISSN: 2411-7986
Baghdad Science Journal

Thus, $\phi^s(L_B)$ is the luminosity function of disc systems which can be written as [15]:

$$\phi^s(L_B) = \phi(L_B) + \phi(L_B^d)\left(\frac{L_B}{L_B^d}\right)^{-2.7} \dots\dots\dots\dots\dots\dots\dots\dots\dots 13$$

A good fit for the disk systems mass function $\psi^{s,B}$ in the blue band is [15]:

$$\Psi^{s,B}[\,in\ Mpc^{-3}M_\odot{}^{-1}] = 1.2x10^{-3}\left[1+\left(\frac{M_b}{M_T}\right)^{-1.46}\right] x\ \left(\frac{M_b}{M_b^d}\right)^{-0.46} e^{-\left(\frac{M_b}{M_b^d}\right)} \dots\dots\dots\dots 14$$

Where $M_b^d = 2.7x10^{11}M_\odot\ and\ M_T = 6.7x10^7\ M_\odot$ [15]

Hence, M_b is the baryonic disk mass, which is the sum of the stellar mass and the gas mass [19, 27]:

$$M_b[in\ M_\odot] = M_* + M_{gas} \dots\dots\dots\dots\dots\dots\dots\dots\dots\dots\dots\dots 15$$

The stellar mass is calculated through [19]:

$$M_*\,[in\ M_\odot] = \Upsilon^{*,B} L_B\, M_\odot / L_\odot = \Upsilon^{*,B} 10^{-0.4(M_B-5.48)} \dots\dots 16$$

where $\Upsilon^{*,B}$ is the stellar population mass-to-light ratio in the Blue-band, the Sun's magnitude in the blue range is "5.48", while M_B is a star's absolute magnitude in the blue band, it is clear that we are talking about stellar emission generated in the 4400 A^0 region of the spectrum, which is considered to be the "blue" regime. The relationship between a galaxy's apparent magnitude, distance, and distance modulus determines its absolute magnitude. As a result, the stellar mass depends on apparent magnitude, distance, and stellar mass-to-light proportion. In this work, the mass-to-light ratios in the blue band for the stellar mass populations of barred and unbarred spiral galaxies are adopted to be $\Upsilon^{*,B} = 1.4\ M_\odot/L_\odot$ [36].

The second term contributing to the baryonic disk systems mass is gaseous disc mass M_{gas}, atomic and molecular gas masses used to compute the total gas mass, which is given by [27, 36-39]:

$$M_{gas}[in\ M_\odot] = 1.33(\,M_{HI} + M_{H2}) \dots\dots\dots 17$$

Helium's impact is considered to have a constant of 1.33. The mass-to-light proportions Υ^* essentially include whatever dark gas emission (whether molecular or ionized gases), provided that it increases alongside M^* [37, 38]. Ionized gas was first discovered using ground-breaking H-emission measurements, but it can be hard to calculate its mass since the HI/HII evolution has an acute point. The current study regards the HII component as baryonic dark matter that is yet unspecified [15, 40-43]. Accordingly, the mass of neutral atomic hydrogen MHI is traced by an emission of 21 cm and is calculated through the followin equation [38, 44-47]:

$$M_{HI} = N_{HI} m_H \dots\dots 18$$

$$M_{HI}[in\ M_\odot] = 2.35x10^5\ d_L^2 S_{HI} \dots\dots\dots 19$$

Where d_L is the luminosity distance in unit (Mpc) collected from NASA/IPAC Extragalactic Database (NED), and S_{HI} is observed frame velocity integrated flux at $\nu_{HI}=1.4GHz$. Here, the number of HI atoms [48], $N_{HI} = \frac{16\pi\, d_L^2\, S_{HI}}{3\, h\nu_{HI} A_{HI}}$ with a spontaneous emission rate of A_{HI}, an emitted photon energy $h\nu_{HI}$, and $m_H = 1.673533\times 10^{-27}\,kg$.

According to HI measurements, atomic gas often dominates *Mg* in disk spiral galaxies. Given a CO-to-H2 transformation component, which could differ from galaxy to galaxy based on metallicity or other features, the molecular hydrogen gas mass could be approximated from CO data. Low-mass, metal-poor disk galaxies frequently exhibit undiscovered carbon monoxide "CO" emissions [37, 40]. Fortunately, molecules often only make up a small portion of their dynamics and motion (fewer than ten per cent of M_b) [40,42]. Thus, the molecular gas mass MH_2 was calculated using the succeeding Eq. 20 if the flux is available at the carbon monoxide line ^{12}CO (J=1-0) in our sample for the barred and unbarred spirals [49-51].

$$M_{H2}[in\ M_\odot] = 3.9x10^{-17}\ \alpha_{CO(1-0)} d_L^2 S_{CO(1-0)} \dots\dots\dots 20$$

where $S_{CO(1-0)}$ is the velocity integrated intensity in unit (Jy km/s) at rest frequency ν_{rest} (^{12}CO =115.27 GHz) selected NED website, and $\alpha_{CO(1-0)}$ is a CO-H_2 conversion factor, in this paper $\alpha_{CO(1-0)} = 2x10^{20} cm^{-2} K\ kms^{-1}$ is used.

The luminosity of the galaxies in the blue-optical band (λ=4400A^0) in unit blue solar luminosity ($L_{B,\odot}$) using an absolute magnitude of the Sun in the blue band $M_{B,\odot} = +5.48^m$ is computed by the method [27,52]:

2024, 21(10): 3277-3288
https://doi.org/10.21123/bsj.2024.10452
P-ISSN: 2078-8665 - E-ISSN: 2411-7986
Baghdad Science Journal

$$L_B\left(L_{B,\odot}\right) = 10^{-0.4(M_B-5.48)} \text{ ……..21}$$

Results and Discussion

This work investigated the multiple regression analysis of values of parameters on the graph for a Schechter function that fits the luminosity function in baryonic disk mass $\psi^S(M_b)$ or in magnitude terms $\emptyset^B(M_B)$ as an expression of absolute magnitude at the blue-band range baryonic mass and luminosity blue-optical $L_{B,\odot}$, calculated in the blue spectrum of the Sun $M_{B,\odot} = +5.48^m$ for barred and unbarred spiral galaxies. Our analysis makes use of the technique created in [15]. This technique has been effectively used for overseeing the subtraction of background information.

Fig. 1 depicts the Schechter function supplied to the luminosity function in absolute magnitude $\emptyset^B(M_B)$ as solid blue lines. The dashed red lines represent the Schechter function fitting to the mass function $\psi^S(M_b)$. To compute the Schechter function for each barred and unbarred spiral Hubble classification, right down to $M_B < -18$, with an exact estimation of the faint-end slope and global normalization. The empirical information is boosted even more by considering the spiral luminosity function, which is constructed from the physical characteristics of the objects instead of their spectral properties. Furthermore, at $M_B < -18$ *mag.*, both the luminosity function $\psi^S(M_b)$and the magnitude measure $\emptyset^B(M_B)$ ignore low-surface luminosity galaxies, representing only a tiny proportion of the total population of disc systems at these luminosities.

The statistical study revealed fairly robust and highly significant relationships between ($\emptyset^B(M_B)$-M_B) with a very robust partial correlation coefficient (R ~0.88) and a very high probability (P ≤10-7) for unbarred spirals with a slope Log $\emptyset^B(M_B)\alpha\ M_B^{0.9}$, while this relation showed good partial correlation (R ~ 0.7) for barred galaxies with a slope Log $\emptyset^B(M_B)\alpha\ M_B^{0.77}$, and displays an extremely strong connection with a correlation coefficient (R~ 1) in the relationship $Log\ \psi^S(M_b)$- M_B with linear regression slope Log $\psi^S(M_b)\alpha\ MB^{0.97}$for barred and $Log\ \psi^S(M_b)\alpha\ M_B^{0.95}$ for unbarred spirals. The slope of the luminosity distribution seems to have a typical magnitude, $M_B < -18$ mag, as it steepens as it approaches the more faint end. The luminosity characteristics continue to be at over several magnitudes higher on this scale before decreasing rapidly at the bright ends $M_B < -18$ *mag.*, which is typically found in both barred and unbarred disk system galaxies.

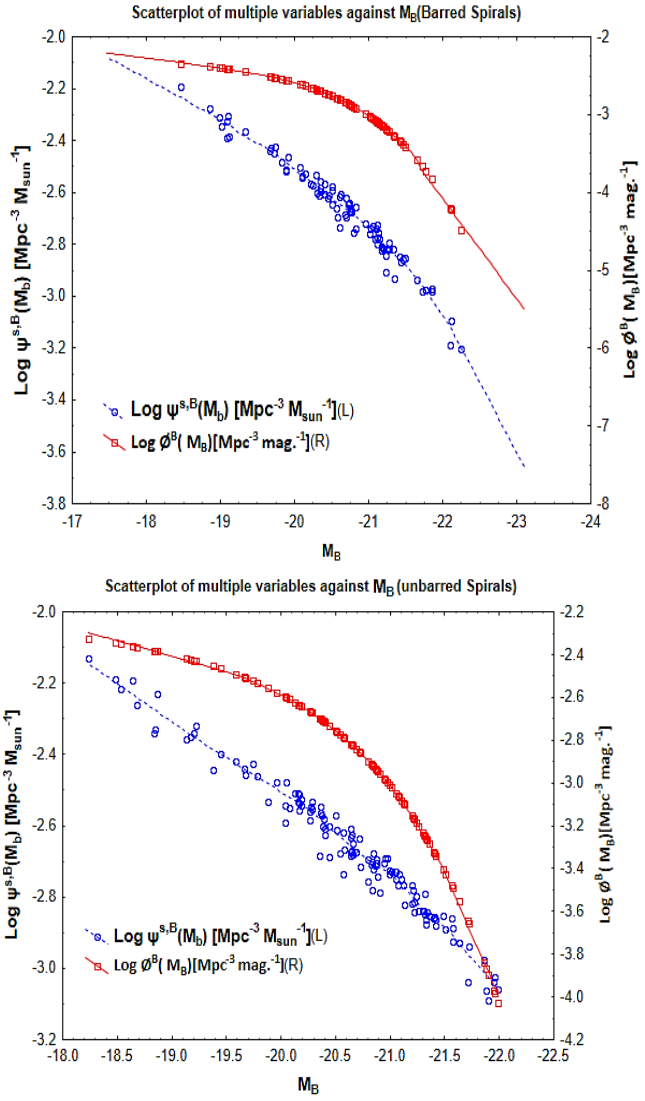

Figure 1. On the right: (Log $\psi^S(M_b)$ and $\emptyset^B(M_B)$) as a function of blue absolute magnitude (M_B) for unbarred spiral galaxies. On the left: (Log $\psi^S(M_b)$ and $\emptyset^B(M_B)$) as a function of (M_B) for barred spiral galaxies.

The mass function exhibits a severe cut-off at the greatest masses, mainly $M_b \approx 6\ x\ 10^{10}\ M_\odot$ for barred and $M_b \approx 3\ x\ 10^{10}\ M_\odot$ for unbarred spirals, the "knee" of the spiral luminosity functions. These lend support to the theory that disk system spirals originated within a higher mass threshold, $M_{bmax} \approx 4x10^{11}\ M_\odot$, $M_{bmin} \approx 4x10^9 M_\odot$ for barred, and $M_{bmax} \approx 2x10^{11}\ M_\odot$,

2024, 21(10): 3277-3288
https://doi.org/10.21123/bsj.2024.10452
P-ISSN: 2078-8665 - E-ISSN: 2411-7986
Baghdad Science Journal

M_{bmin} $\approx 5x10^{9} M_{\odot}$ for unbarred, owing to the impossibility of a greater baryonic mass to cool quickly enough to settle into a disk during a Hubble timescale. Considering that the emitting brightness of stellar discs of certain masses has a substantial spread caused by variances in the disk's stellar populations in general, this strong cut-off broadens the luminosity function (Fig. 2).

In the current study, it has been also explored the relationships between baryonic mass (M_b) disk spiral systems and luminosity function in baryonic disk mass $\psi^{S}(M_b)$ or magnitude units $\emptyset^{B}(M_B)$. The results additionally indicated a very strong partial correlation between the associations of Log $\psi^{S}(M_b)$ and $LogM_b$, with a tight correlation coefficient (R) of -0.96 and a slope line of ~ -1 for barred disc galaxies; furthermore, the relationship between Log $\emptyset^{B}(M_B)$ and $LogM_b$ has R-value of - 0.7 with a regression value of (Log $\emptyset^{B}(M_B)$ α $LogM_b^{-0.76}$) for barred disc galaxies, the probability of a very robust chance (P $\leq$10-7) for two cases. According to statistics, we infer that Log $\psi^{S}(M_b)$ and $LogM_b$ have a linear connection (*Slope* ~ -1). Our analysis additionally demonstrates the presence of a very close relationship between the logarithmic scales $\psi^{S}(M_b)$ and M_b with a partial coefficient correlation ($R \approx$ -1) and the relationship between Log $\emptyset^{B}(M_B)$ and $LogM_b$ with an R-value of - 0.86 and a regression coefficient of (Log $\emptyset^{B}(M_B)\alpha$ $LogM_b^{-0.9}$) for unbarred galaxies with Slope ~ -1 (see Fig. 2). The general form of the luminosity function varies regularly as baryonic mass increases. All of the evidence shows that when baryonic mass increases, the proportion of the initial luminosity function decreases. The structure, nevertheless, transforms when centrals are taken into account, demonstrating that centrals are the predominant component of lower-mass baryonic. We observe that for baryons with $M_b > 10^{10} M_{\odot}$ in both cases barred and unbarred, the overall fit significantly underestimates the luminous ends of the luminosity function. This is caused by using a constant M_b for all masses (gases + stars). It is possible to see bars in the disk system spiraling on just one side of the nucleus, with the other half being either dim or missing. One often observes regions of increasing luminosity in loops or super relationships, which are almost certainly the locations of star formation at the ends of bars. The existence of a bar influences a variety of processes that take place in disk spiral galaxies. Keep in mind the major role that bars play in the numerous phenomena seen in disk galaxies. For barred spiral galaxies, hydrogen gas flows toward the galaxy's Centre, causing a burst of stars that results in a gradual decline. In contrast, in unbarred galaxies, the generation of star fraction increases steadily and continuously. Unbarred galaxies have a substantially lower active nucleus illumination than barred galaxies, and their inner regions include a smaller amount of gas that can be influenced by interaction.

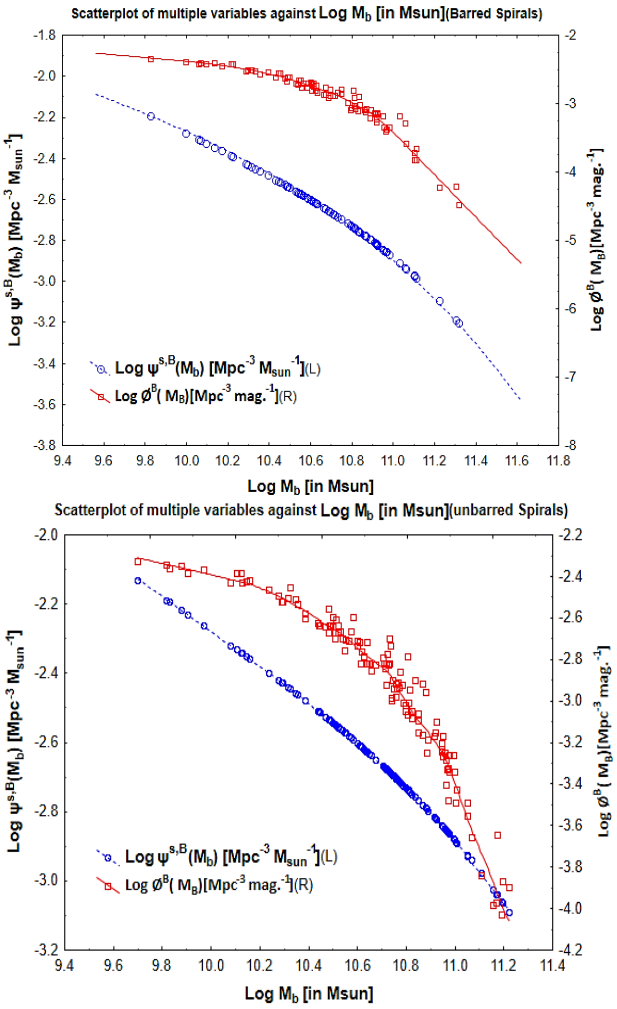

Figure 2. On the right: (Log $\psi^{S}(M_b)$ and $\emptyset^{B}(M_B)$) as a function of the baryonic mass disk system (M_b) for unbarred spiral galaxies. On the left: (Log $\psi^{S}(M_b)$ and $\emptyset^{B}(M_B)$) as a function of baryonic mass disk system (M_b) for barred spiral galaxies

Fig. 3 describes the relationship between the initial mass function $\psi^{S}(M_b)$and the number density of stars with absolute magnitude $\emptyset^{B}(M_B)$ and luminosity blue-optical $L_{B,\odot}$ determined in the blue part of these galaxies, which shows the existence of a very significant relation $Log\ \psi^{S}(M_b)$-$Log\ L_{B,\odot}$ with a negative correlation coefficient (R ~ - 0.93) for barred spirals, whereas an extremely high correlation

2024, 21(10): 3277-3288
https://doi.org/10.21123/bsj.2024.10452
P-ISSN: 2078-8665 - E-ISSN: 2411-7986
Baghdad Science Journal

(R ~ -1) for the unbarred spiral galaxies with a significantly steep probability ($P \leq 10^{-7}$) in the two cases. It is very important to note that the slope of the line is linear and equal to minus one ($(Log\ \psi^S(M_b)\ \alpha\ Log\ L_{B,\odot}{}^{-0.97}$ for barred and $Log\ \psi^S(M_b)\ \alpha\ Log\ L_{B,\odot}{}^{-0.95}$ for unbarred). For barred galaxies, there is a substantial connection between Log $\emptyset^B(M_B)$ and $Log\ L_{B,\odot}$, with an acceptable partial correlation (R ~ - 0.7) and a perfect importance probability ($P \leq 10^{-7}$) and a slope line of ~ - 0.8, and for unbarred spirals, there is a robust correlation between Log $\emptyset^B(M_B)$ and Log $L_{B,\odot}$, with R ~-0.87 and a slope line of -0.9. We study disk systems with luminosities ranging from $L_B{}^{max} \approx 3x10^{11}\ L_{B,\odot}$ to $L_B{}^{min} \approx 2x10^9\ L_{B,\odot}$ for barred, $L_B{}^{max} \approx 10^{11}\ L_{B,\odot}$ and $L_B{}^{min} \approx 3x10^9\ L_{B,\odot}$ for unbarred. In the case of an energy bandwidth, Fig. 3 depicts the development of the comoving galaxies' luminosity distribution with luminosity blue-optical. For both barred and unbarred disk galaxies, we can observe that the knee of the luminosity function shifted in earlier times in favor of higher luminosities. As a consequence, the connection that exists between the amount of initial mass function $\psi^S(M_b)$, the number density of stars with absolute magnitude $\emptyset^B(M_B)$ and the blue luminosity of our sample galaxies barred and unbarred are complicated, unstable, and dependent on a wide range of external as well as internal variables, involving the environment, illumination, construction, and the place of creation of stars operation, accordingly.

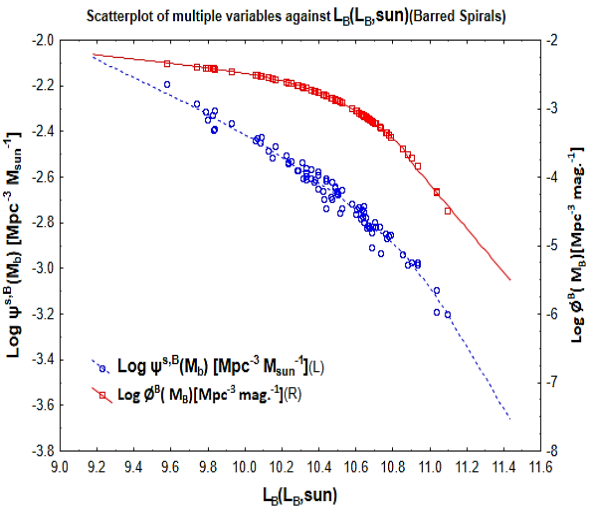

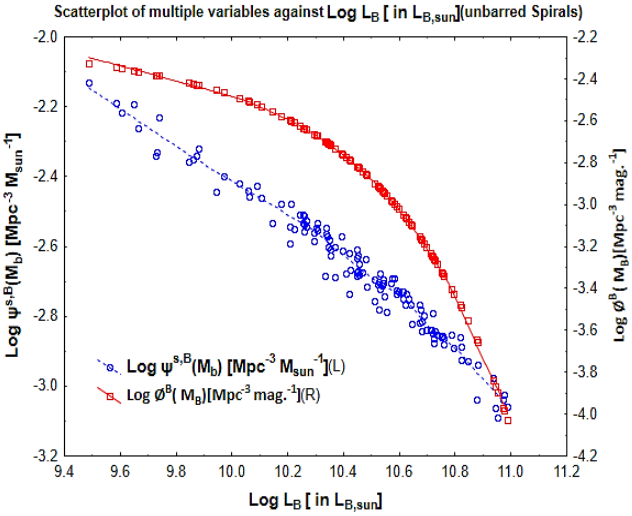

Figure 3. On the right: (Log $\psi^S(M_b)$ and $\emptyset^B(M_B)$) as a function of blue luminosity (Log L_B) for unbarred spiral galaxies. On the left: (Log $\psi^S(M_b)$ and $\emptyset^B(M_B)$) as a function of (Log L_B) for barred spiral galaxies.

We additionally analyze the evolution of the initial mass function $\psi^S(M_b)$with redshift z, as shown in Fig. 4. The initial mass functions have distinct structures primarily determined by the history of the star's creation. In the past, the luminosity function in baryonic disk mass declined because the mass fraction inside galaxies decreased and their star population reduced. The growth of the stellar initial mass function with redshift is substantially slower, implying that the diminution of the comoving initial mass function of barred and unbarred galaxies at high redshift is less than for the crucial universe ($z > 0.027$ for barred and $z > 0.02$ for unbarred). Its reduction in past times is attributable to two factors. Initially, we look at baryons with a high-temperature $T > 10^4\ K^0$ "cutoff caused by poor cooling", resulting in a reduced initial mass fraction there was less mass held in profoundly likely drilling in earlier times. In addition, at higher redshifts, galaxies have a higher gas/star content proportion (smaller time-scale $t_0\ \alpha\ (1+z)^{-3/2}$), implying that most of the mass is in the state of the gas.

2024, 21(10): 3277-3288
https://doi.org/10.21123/bsj.2024.10452
P-ISSN: 2078-8665 - E-ISSN: 2411-7986
Baghdad Science Journal

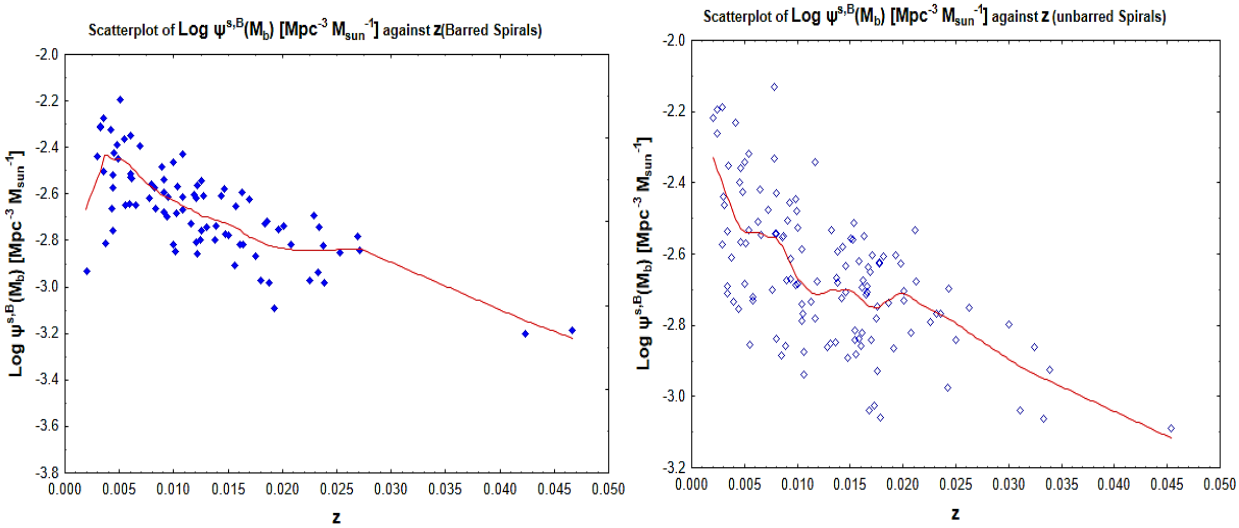

Figure 4. On the right: Log $\psi^S(M_b)$ as a function of redshift (z) for unbarred spiral galaxies. On the left: Log $\psi^S(M_b)$ as a function of redshift (z) for barred galaxies.

Conclusion

This study estimated the luminosity function in terms of baryonic disc mass $\psi^S(M_b)$, magnitude $\emptyset^B(M_B)$, baryonic disc mass and luminosity blue-optical. Our major conclusions may be summed up as: On a range of magnitudes, the luminosity features are still many magnitudes higher before sharply declining at the brilliant ends. Both barred and unbarred disc system galaxies generally have $M_B < -18$ mag. The "knee" of the spiral brightness function, $M_b \approx 6 \times 10^{10}\ M_\odot$ for barred spirals and $M_b \approx 3 \times 10^{10}\ M_\odot$ for unbarred spirals, is where the mass function shows a significant cut-off value. The general fit seems to severely undervalue the luminous ends of the luminosity function for baryons with $M_b > 10^{10}\ M_\odot$ in both barred and unbarred configurations. This results from using a fixed Mb value for all abundance gases and stars. The knee of the luminosity operation has shifted earlier to support greater brightness for both barred and unbarred disc galaxies. As a result, the relationship between the quantity of the initial mass function $\psi^S(M_b)$, the number density of stars with absolute magnitude $\emptyset^B(M_B)$, and the blue luminosity of our sample galaxies, barred and unbarred, is complex, unsteady and reliant on a wide range of external as well as internal variables, involving the surroundings, lighting, development, and the location of the stars' formation, respectively. Finally, it implied that the comoving initial mass function $\psi^S(M_b)$ of barred and unbarred galaxies at high redshift ($z > 0.027$ for barred and $z > 0.02$ for unbarred) is less diminished than for the crucial universe because the increase of the star initial mass function with redshift is significantly quicker. Galaxies with larger redshifts have a larger star-to-gas ratio (short time scale $t_0 \alpha\ 1/(1+z)^{3/2}$), indicating that most of the mass is in gaseous form.

Acknowledgment

We are appreciative to the Special Astrophysical Observatory (Russia), HyperLEDA (De Lyon, France), and the NASA/IPAC Extragalactic Database "NED" for offering the unique data sets of the spiral extragalactic. We appreciate the anonymous referee's numerous perceptive remarks, greatly enhancing the work.

Authors' Declaration

- Conflicts of Interest: None.
- We hereby confirm that all the Figures and Tables in the manuscript are ours. Furthermore, any Figures and images, that are not ours, have been included with the necessary permission for re-publication, which is attached to the manuscript.

- Ethical Clearance: The project was approved by the local ethical committee at University of Baghdad.

Authors' Contribution Statement

M. N. A., Y. E. R., and H. H. A. contributed to proposing the title and idea of the manuscript, and they equally to writing the manuscript after discussing each step and analyzing the results.

References

1. Jesús FB, Johan HK. Secular Evolution of Galaxies. 2nd ed. New York: Cambridge University Press; 2013. 179. https://doi.org/10.1017/CBO9781139547420
2. Aleksandr VM, Andrey DP, Savanah T, Bartier CL, Maria NS, Alexander AM, et al. A multiwavelength study of spiral structure in galaxies. II. Spiral arms in deep optical observations. Mon Notices Royal Astron Soc. 2023; 527: 10615–10631. https://doi.org/10.1093/mnras/stad3869
3. Al-Ramahi FKM. Spatial analysis of radon gas concentration distrbuted at Baghdad city using remote sensing and geographic information system techniquesd. Iraqi J Agric Sci. 2020; 51: 21–32. https://doi.org/10.36103/ijas.v51iSpecial.879
4. Eskridge PB, Frogel JA, Pogge RW, Quillen AC, Davies RL, DePoy DL, et al. The Frequency of Barred Spiral Galaxies in the Near-Infrared. Astron J. 2000; 119(2): 536-544. https://doi.org/10.1086/301203
5. Raaid NH, Huda ShA, Wafaa HW. Computer Simulation for the Effects of Optical Aberrations on Solar Images Using Karhunen-Loeve polynomials. Iraqi J Sci. 2021; 62(7): 2463-2473. https://doi.org/10.24996/ijs.2021.62.7.35
6. Ramin AS, Karen LM, Robert CN, Idit Z, Ben H, Edward ME, et al. Galaxy Zoo: the environmental dependence of bars and bulges in disc galaxies Mon Notices Royal Astron Soc. 2012; 423: 1485–1502. https://doi.org/10.1111/j.1365-2966.2012.20972.x
7. Abdullah KA. Comparison of the Structure of Spiral and Lenticular Galaxies, NGC 4305 and NGC 4203 as a Sample. Iraqi J Sci. 2023; 64(4): 2051–2059. https://doi.org/10.24996/ijs.2023.64.4.39
8. Ahmed HA, Pavel K. Specific Frequency of Globular Clusters in Different Galaxy Types. Int J Phys Math Sci. 2018; 12(9): 190-195. https://doi.org/10.5281/zenodo.1474591
9. Andreani P, Miyamoto Y, Kaneko H, Boselli A, Tatematsu K, Sorai K, et al. The molecular mass function of the local Universe. Astron. Astrophys. 2020; 643: L11. https://doi.org/10.1051/0004-6361/202038675
10. Johnston R. Shedding light on the galaxy luminosity function. Astron Astrophys Rev. 2011; 19: article id.41. https://doi.org/10.1007/s00159-011-0041-9
11. Al Najm MN, Polikarpova OL, Shchekinov YuA. Ionized Gas in the Circumgalactic Vicinity of the M81 Galaxy Group. Astron Rep. 2016; 60(4): 389-396. https://doi.org/10.1134/S106377291603001X
12. Rashed YE, Al Najm MN, Al Dahlaki HH. Studying the Flux Density of Bright Active Galaxies at Different Spectral Bands. Baghdad Sci J. 2019; 16(1) Supplement: 30-236. https://dx.doi.org/10.21123/bsj.2019.16.1
13. Al Najm MN, Mahdi HS, Abdullah SA. The Exponential and Gaussian Density Profiles of HI and Fe II in the Gaseous Halo of the Milky Way. Iraqi J Sci. 2017; 58(4C): 2467-2472. https://ijs.uobaghdad.edu.iq/index.php/eijs/article/view/98
14. Maha AH, Saif BAl-Khoja, Rafah RI. Small Binary Codebook design depending on Rotating Blocks. Iraqi J Sci. 2021; 62(10): 3719-3723. https://doi.org/10.24996/ijs.2021.62.10.30
15. Salucci P, Persic M. The baryonic mass function of spiral galaxies: clues to galaxy formation. Mon Notices Royal Astron Soc. 1999; 309: 923 -928. https://doi.org/10.1046/j.1365-8711.1999.02913.x
16. Shankar F, Salucci P, Danese L. The Baryonic vs Dark Matter Halo Mass Relationship in Galaxies: the effect of the inefficiency of the Cosmolog. star formation. PoS Proc Sci. 2004 ; 14: id 59. https://doi.org/10.22323/1.014.0059
17. Read JI, Neil T. The baryonic mass function of galaxies. Phil Trans R Soc A. 2005; 363(1837): 2693–2710. https://doi.org/10.1098/rsta.2005.1648
18. Kevin RC, Suzanne LH, John JB, Andrew AW, Reid IN, David AG, et al. The Luminosity and Mass Functions of Low-Mass Stars in the Galactic Disk. I. The calibration region. Astron J. 2008; 136: 1778–1798, https://doi.org/10.1088/0004-6256/136/5/1778
19. Trachternach C, de Blok WJG., McGaugh SS, van der Hulst JM, Dettmar RJ. The baryonic Tully-Fisher relation and its implication for dark matter halos. Astron Astro phys. 2009; 505: 577–587. https://doi.org/10.1051/0004-6361/200811136
20. Amanda RL, Alvaro I, Marcelo BR, William RS. Galaxy cosmological mass function Galaxy cosmological mass function. Astron Astrophys. 2014; 572: A27. https://doi.org/10.1051/0004-6361/201423445
21. Hunt LR, Pisano DJ, Crawford SM, Bershady MA, Wirth GD. The Evolution of the Luminosity Function for Luminous Compact Blue Galaxies to z=1.

Astrophys J. 2021; 909: 49 (12pp). https://doi.org/10.3847/1538-4357/abda4c
22. Steer I, Madore BF, Mazzarella JM, Schmitz M, Corwin HG, Chan BHP, et al. Redshift-Independent Distances in the NASA/IPAC Extragalactic Database: Methodology, Content, and Use of NED-D. Astron J. 2017; 153(1): article id. 37. https://doi.org/10.3847/1538-3881/153/1/37
23. Ahmed HA, Pavel K. The Dichotomy of the Mass-radius Relation and the Number of Globular Clusters. Astron Lett. 2021; 47: 170–174. https://doi.org/10.1134/S1063773721030014
24. Al-baqir HR, Abdullah KA, Gamal D. Surface Photometry of NGC 3 Lenticular Galaxy. Iraqi J Sci. 2019; 60(9): 2080–2086. https://doi.org/10.24996/ijs.2019.60.9.23
25. Dmitry M, Philippe P, Nataliya T, Hélène C, Isabelle V. HyperLEDA. III. The catalogue of extragalactic distances. Astron Astrophys. 2014; 570: A13. https://doi.org/10.1051/0004-6361/201423496
26. Maha MZ, Al Najm MN. Computation of the Relationships of X-ray to Radio Luminosities of a Sample of Starburst Galaxies. Iraqi J Sci. 2023; 64(6): 4076-4093. https://doi.org/10.24996/ijs.2023.64.6.44
27. Al Najm MN, AL-Dahlaki HH, Alkotbe BA. Investigation of the Baryonic Mass Tully–Fisher Relationship for Normal and Barred Spiral Galaxies. Iraqi J Sci. 2023; 64(12): 6620-6637. https://doi.org/10.24996/ijs.2023.64.12.41
28. Rasha HI, Abdul-Rahman HS. A comparison between Runge-Kutta and Adems-Bashforth methods for determining the stability of the satellite's orbit. AIP Conf Proc. 2020; 2290(1). https://doi.org/10.1063/5.0027420
29. Albakri SAA, Abdul Hussien MN, Herdan H. Measurement of the distance to the central stars of Nebulae by using Expansion methods with Alladin Sky Atlas. IOP Conf Ser Mater Sci Eng. 2020; 757. https://doi.org/10.1088/1757-899X/757/1/012043
30. Rashed YE, Eckart A, Valencia MS., García-Marín M, Busch G, Zuther J, et al. Line and continuum variability in active galaxies. Mon Notices Royal Astron Soc. 2015; 454 (3): 2918–2945. https://doi.org/10.1093/mnras/stv2066
31. Zahraa A, Abdullah KA. Surface Photometry of Spiral Galaxy NGC 5005 and Elliptical Galaxy NGC 4278. Baghdad Sci. J. 2018; 15(3): 314-323. https://doi.org/10.21123/bsj.2018.15.3.0314
32. Massimo P, Paolo S. The baryon content of the Universe. Mon Notices Royal Astron Soc. 1992 Sep 01; 258: 14-18. https://doi.org/10.1093/mnras/258.1.14P
33. Schneider P. Extragalactic Astronomy and Cosmology an Introduction. Second Edition. New York: Springer Berlin Heidelberg; 2015. 155p. https://doi:10.1007/978-3-642-54083-7
34. Favole G, Gonzalez-Perez V, Ascasibar Y, Corcho-Caballero P, Montero-Dorta AD, Benson AJ, et al., Characterizing the ELG luminosity functions in the nearby Universe. arXiv: 2303.11031. astro-ph. GA. https://doi.org/10.48550/arXiv.2303.11031
35. Ryou Oh, Takashi O, Chikako Y. Impact of the initial disk mass function on the disk fraction. Publ Astron Soc Jpn. 2015; 67 (6): 120 (1–9). https://doi.org/10.1093/pasj/psv094
36. McGaugh SS, Schombert JM, Bothun GD, de Blok WJG. The Baryonic Tully-Fisher Relation. Astrophys J. 2000; 533: L99–L102. https://doi.org/10.1086/312628
37. Federico L, McGaugh SS, Schombert JM. The Small Scatter of the Baryonic Tully–Fisher Relation. Astrophys J Lett. 2016; 816: L14 (6pp). https://doi.org/10.3847/2041-8205/816/1/L14
38. McGaugh SS, Schombert JM. Weighing Galaxy Disks with the Baryonic Tully–Fisher Relation. Astrophys J. 2015; 802:18 (16pp). https://doi.org/10.1088/0004-637X/802/1/18
39. Dua'a KA, Al Najm MN. Investigation of the Characteristics of CO (1-0) Line Integrated Emission Intensity in Extragalactic Spirals. Iraqi J Sci. 2022; 63(3): 1376–1393. https://doi.org/10.24996/ijs.2022.63.3.39
40. Andreas S, Adam KL, Fabian W, Frank B, Elias B, de Blok WJG, et al. Low CO Luminosities in Dwarf Galaxies. Astron J. 2012; 143: 138 (18pp). https://doi.org/10.1088/0004-6256/143/6/138
41. Julian SG, David VS, Karen LM, Kevin B, Niv D, David RL. A comparison of the baryonic Tully–Fisher relation in MaNGA and IllustrisTNG. Mon Notices Royal Astron Soc. April 2023 Feb 02; 520(3): 3895–3908. https://doi.org/10.1093/mnras/stad298
42. Meza A, Lipovka AA. Modeling the Rotation Curve of Disk Galaxies. Astrophys Bull. 2022; 77(2): 123-131. https://doi.org/10.1134/S1990341322020055
43. Kenji B. A mechanism of bar formation in disc galaxies: Synchronization of apsidal precession. Mon Notices Royal Astron Soc. 2023; 523(4): 5823–5840. https://doi.org/10.1093/mnras/stac3097
44. Xingchen L, Isaac Sh, Daniel P, Clayton H. The origin of buckling instability in galactic bars: Searching for the scapegoat. Mon Notices Royal Astron Soc.2023; 520(1): 1243–1257. https://doi.org/10.1093/mnras/stad076
45. McGaugh SS. The Baryonic Tully-Fisher Relation of Galaxies with Extended Rotation Curves and the Stellar Mass of Rotating Galaxies. Astrophys J. 2005; 632: 859–871. https://doi.org/10.1086/432968
46. Federico L. Gas dynamics in dwarf galaxies as testbeds for dark matter and galaxy evolution. Nature Astron. 2022; 6: 35–47. https://doi.org/10.1038/s41550-021-01562-2
47. Justin HR, Misty CB, Hélène MC, Megan CJ, Crenshaw DM, Beena M, et al. Tully–Fisher Distances and Dynamical Mass Constraints for 24

2024, 21(10): 3277-3288
https://doi.org/10.21123/bsj.2024.10452
P-ISSN: 2078-8665 - E-ISSN: 2411-7986
Baghdad Science Journal

Host Galaxies of Reverberation-mapped AGNs. Astrophys J. 2021; 912 (2): 160. https://doi.org/10.3847/1538-4357/abedaa
48. Martin M, Aaron R, Danail O, Tobias W, Alan D, Lister SS. Tracing HI Beyond the Local Universe. Publ Astron Soc Aust. 2017; 34(52): 12pages. https://doi.org/10.1017/pasa.2017.31
49. Al Najm MN. Studying the Atomic and Molecular Hydrogen Mass (MHI, MH2) Properties of the Extragalactic Spectra. Iraqi J Sci. 2020; 61(5): 1233-1243. https://doi.org/10.24996/ijs.2020.61.5.30
50. Herrero-Illana R, Privon GC, Evans AS, Díaz-Santos T, Pérez-Torres MÁ, Vivian U, et al. Molecular gas and dust properties of galaxies from the Great Observatories All-sky LIRG Survey. Astron Astro phys. 2019; 628: A71. https://doi.org/10.1051/0004-6361/201834088
51. Hiroyuki K, Shoya T, Nario K. Investigating physical states of molecular gas in the overlapping region of interacting galaxies NGC 4567/4568 using ALMA. Publ Astron Soc Jpn. 2023; 75(3): 646–659. https://doi.org/10.1093/pasj/psad025
52. Bradley WC, Dale AO. An Introduction to Modern Astrophysics. 2nd ed. Pearson Education; Inc., Addison-Wesley: 2007. 973p. https://doi.org/10.1017/9781108380980

مقارنة الخصائص الفيزيائية لدالة الكتلة والضيائية لأنظمة الأقراص في المجرات الحلزونية القضيبية وغير القضيبية

محمد ناجي ال نجم ، ياسر عز الدين رشيد ، حسنين حسن الدهلكي

قسم الفلك والفضاء ، كلية العلوم ، جامعة بغداد ، بغداد ، العراق.

الخلاصة

إحدى أهم الطرق لتقصي توزيع المجرات عبر الزمن الكوني هي دالة اللمعان LF بدلالة كتلة القرص الباريوني $\psi^S(M_b)$، القدر $\emptyset^B(M_B)$. لقد درسنا تقديرًا لكثافة كتلة الباريون في عينة من المجرات الحلزونية القضيبية وغير القضيبية من الادبيات السابقة، والتي تتضمن فعليًا، لكل صنف من الاجرام السماوية ذات المحتوى الباريون المرئي، جزءًا لا يتجزأ من ناتج دالة الضيائية (LF) ونسبة الكتلة إلى الضوء. استخدمت تقنية الانحدار المتعدد لحزمة البرامج الإحصائية في دراستنا ونتائجنا، مثل برنامج تحليل قواعد البيانات والرسوم البيانية(برامج Origin Pro و Statistics Win) . وفقًا للتحليل الإحصائي، هناك علاقة إيجابية قوية وارتباط وثيق للغاية $(\emptyset^B(M_B), \psi^S(M_b) \alpha\ M_B^{\sim 1})$ ، وغالبًا ما تظهر المجرات الحلزونية القرصية القضيبية وغير القضيبية قدراً مطلقاً بحدود M_B < -18 mag . "الركبة" لدالة الضيائية للمجرات الحلزونية تبين قطعًا كبيرًا عند كتلة باريونية تبلغ $M_b > 10^{10}\ M_\odot$ للمجرات الحلزونية القضيبية وغير القضيبية. يوفر هذا دليلاً يدعم الفرضية القائلة بأن اللوالب الحلزونية لنظام القرص بدأت تتشكل داخل عتبة كتلة متزايدة. نظرًا لأن زيادة دالة الكتلة الأولية للنجم مع الانزياح نحو الأحمر تكون أسرع بكثير، فقد أشارت النتائج التي توصلنا إليها إلى أن دالة الكتلة الأولية المنتقلة $\psi^S(M_b)$ للمجرات القضيبية وغير القضيبيةعند انزياح أحمر مرتفع $z > 0.027$ للمجرات االقضيبية و $z >$ 0.02للمجرات غير القضيبية والذي يبدو أنه يتناقص مقارنة بالكون الحرج.

الكلمات المفتاحية: الكتلة الباريونية ، دالة الضيائية ، دالة الكتلة الاولية ، المجرات ذات النوع الحلزوني ، الغاز الذري والجزيئي.